Rock and Soil Mechanics

Volume 44 | Issue 4 Article 7

7-19-2023

Numerical study on failure path of rock slope induced by multi-stage excavation unloading based on crack propagation

Chuan WANG
State Key Laboratory of Geomechanics and Geotechnical Engineering, Institute of Rock and Soil Mechanics, Chinese Academy of Sciences, Wuhan, Hubei 430071, China, University of Chinese Academy of Sciences, Beijing 100049, China

Xian-lun LENG
State Key Laboratory of Geomechanics and Geotechnical Engineering, Institute of Rock and Soil Mechanics, Chinese Academy of Sciences, Wuhan, Hubei 430071, China, University of Chinese Academy of Sciences, Beijing 100049, China

Zhan-rong ZHANG
China Railway Siyuan Survey and Design Group Co., Ltd., Wuhan, Hubei 430063, China

Chuang YANG
China Railway Siyuan Survey and Design Group Co., Ltd., Wuhan, Hubei 430063, China

See next page for additional authors

Numerical study on failure path of rock slope induced by multi-stage excavation unloading based on crack propagation

Authors

Chuan WANG, Xian-lun LENG, Zhan-rong ZHANG, Chuang YANG, and Jian CHEN

Rock and Soil Mechanics 2023 44(4): 1190−1203 ISSN 1000−7598
https: //doi.org/10.16285/j.rsm.2022.5667 http://rocksoilmech.researchcommons.org/journal

Numerical study on failure path of rock slope induced by multi-stage excavation unloading based on crack propagation

WANG Chuan[1, 2], LENG Xian-lun[1, 2], ZHANG Zhan-rong[3], YANG Chuang[3], CHEN Jian[1, 2]

1. State Key Laboratory of Geomechanics and Geotechnical Engineering, Institute of Rock and Soil Mechanics, Chinese Academy of Sciences, Wuhan, Hubei 430071, China

2. University of Chinese Academy of Sciences, Beijing 100049, China

3. China Railway Siyuan Survey and Design Group Co., Ltd., Wuhan, Hubei 430063, China

Abstract: The investigation on failure patterns and paths of cracked rock slopes under excavation unloading is one of the hot issues in the slope engineering field. Accurate identification of the potential failure path is of great significance for excavation safety and support design of the slope. A theoretical method for crack propagation discrimination was embedded into the numerical simulation based on the fracture propagation analysis method, and the quick simulation of initiation, propagation, and coalescence of discontinuous cracks in rock masses was realized through stress intensity factor calculation at crack tip, crack propagation pattern recognition, crack initiation angle derivation, and crack propagation and coalescence. The proposed simulation method was used to analyze the crack propagation mechanism and the failure path of a highway cutting slope under multi-stage excavation unloading. The results show that during the multi-stage excavation from top to bottom of the slope, the crack initiation first occurs at the bench edge, and then a dominant propagating crack is formed through tensional propagation. With the downward excavation of the slope, the dominant crack gradually propagates downward the slope in tensile-shear mixed pattern and coalesces with existing cracks, forming a step-path failure in the middle and upper parts of the slope. When the crack propagates to the lower part of the slope, the crack propagation pattern transforms from tensile-shear mixed pattern to shear pattern, and finally the potential sliding body slides out along an arched shear surface at the slope toe. This study reveals a composite failure pattern of the cracked rock slope under multi-stage excavation unloading, which includes the tensile-shear mixed propagation pattern with a step-shaped path in the upper part and the shear propagation pattern with an arched path in the lower part, and can provide new ideas for the support design and construction stability control of rock slopes.

Keywords: crack propagation; excavation unloading; propagation pattern; failure path; cracked rock slope

1 Introduction

Cracks widely exist in rock slopes and play an essential role in slope deformations and failures induced by excavation unloading. The deformation and failure of cracked rock slope is closely related to crack propagation and evolution[1], and the corresponding processes are characterized by crack tension and slide, crack initiation and propagation in rock bridges, and formation of interconnected failure surfaces[2−3].

In the early stages of examining the stability of cracked rock slopes, the limit equilibrium method and the strength reduction method were frequently employed, but these approaches fall short in capturing the intricate propagation and evolution processes of discontinuous cracks in rock bridges and the asynchronous strength weakening effects of rock masses[3, 5]. The stability of rock slope caused by crack evolution was then gradually examined using numerical methods such as the boundary element method[6], the numerical manifold method[7], the discrete element method[8], the extended finite element method[5], and the continuous-discrete coupling method[9]. By introducing a smooth plane and improving the contact model in the discrete element method, Scholtès et al.[10−11] and Jiang et al.[12] were able to simulate the slide and propagation of cracks as well as the crack processes of rock bridge in cracked rock slope. They then analyzed the characteristics of crack initiation and propagation as well as the weakening of rock bridge strength under critical gravity and concluded that the step-shaped failure of cracked rock slope results from crack propagation and coalescence in rock bridge in the form of wing crack. Using the particle discrete element method, Huang et al.[3] and Zhu et al.[13] simulated three failure patterns of rock bridge with different discontinuous crack distribution patterns, including shear failure, tensile failure, and tensile-shear mixed failure. They took into account that the coalescence of discontinuous cracks occurs gradually from the bottom to the top of the slope under gravity and came to the conclusion that the step-shaped failure evolution of the slope can be divided into four stages: elastic deformation, rock bridge failure at the

Received: 7 May 2022 Accepted: 19 June 2022
This work was supported by the National Natural Science Foundation of China (52079135) and the Research Project of Tisiyuan (2020K043).
First author: WANG Chuan, male, born in 1994, PhD candidate, research interests: majoring in rock mechanics and slope stability.E-mail: 1073642650@qq.com
Corresponding author: LENG Xian-lun, male, born in 1980, PhD, Associate Professor, research interests: rock engineering and its stability. E-mail: xlleng@whrsm.ac.cn

slope bottom, upward progressive failure of rock bridge, and whole slide of slope. There are still several limitations to the study presented above, despite its importance in illuminating the failure process of cracked rock slopes. When utilizing the discrete element approach to analyze the failure of a cracked rock slope, it might be challenging to select parameters whose physical implications are not sufficiently clear[11−12]. The boundary element approach, the numerical manifold method, and the extended finite element method are challenging to model complicated fracture networks[5−7]. In order to better understand the processes of crack tension and slide as well as crack initiation and propagation in rock bridge, the analysis and simulation methods for crack propagation were applied to analysis on cracked rock slope[14−15].

Tharp and Coffin[16], Singh and Sun[17], and Scavia[18] attempted to apply fracture mechanics, which is based on solid fracture mechanics, to analyze the stability of cracked rock slopes. They believed that the fracture mechanics method was suitable for analyzing the slope stability impacted by crack propagation and evolution by comparing analytical results with field observation results. Subsequently, the theoretical and numerical methods for crack propagation analysis in rock masses have therefore been quickly developed. Kemeny[19] used the theoretical method to examine the crack tip's weakening characteristics and concluded that the major cause of the early sluggish growth of cracks in rock bridges and the subsequent fast development of cracks in rock bridges is the weakening of crack strength. Chen and Wang[15] used the displacement extrapolation method to analyze the stress intensity factors at the tip of tensile cracks at the back of slopes with different slope shapes, and put forward a fracture mechanics model for the propagation and evolution of tensile cracks. Chen et al.[20] and Zhou[21] deduced a dominantly controlling structural plane model of slope with complex stress intensity factor as the index, and thought that the failure patterns such as slope collapse, fall, and toppling caused by fracture and propagation of the dominantly controlling structural plane could be uniformly classified as compressive-shear fracture or tensile-shear fracture. Gao et al.[22] proposed an energy criterion of crack initiation, and demonstrated the applicability of criterion in slope crack propagation analysis by comparison with an engineering case. Chang et al.[23] derived the analytical expression of crack length, dip angle, and ultimate bearing capacity of slope based on the propagation and evolution characteristics of crack under loading and unloading. Zhou and Chen[24] deduced the interaction coefficient of parallel offset double cracks based on the superposition principle, and improved the fracture criterion in the extended finite element method to simulate the evolution process of crack propagation under the step-shaped failure pattern of inclined rock slope. Haeri et al.[25] simulated the process of crack propagation and coalescence in slope by using the high-order displacement discontinuity method based on fracture propagation criterion, and suggested that the crack inclination angle and slope angle had an important influence on the type of rock bridge failure and the failure path of slope. Aliha et al.[26] analyzed the I/II mixed propagation process of cracks in typical cracked rock slopes by using the maximum shear stress criterion, and thought that the stress at the crack tip had a significant influence on the crack propagation path and the final failure pattern of the slope. Zhang et al.[27] constructed a new joint element combining solid and interface, and simulated the failure evolution process of rock slope including stress concentration at crack tip, crack initiation and propagation of rock bridge, slip weakening of crack surface, and coalescence of fracture surface in rock bridge based on fracture propagation criterion. The crack propagation and coalescence mechanism under the typical rock slope crack distribution is further revealed by the aforementioned analytical and numerical calculations based on fracture mechanics. The interaction between the crack network and the rock bridge, the assessment of the pattern of crack propagation, the judgment of crack propagation pattern, the treatment of crack intersection, and the analysis of slope fracture path all require additional research due to the complexity and dynamic nature of crack propagation in slopes.

Based on the theoretical method of fracture propagation analysis, the deformation and failure evolution process of a rock slope with a complex crack network was simulated using an equivalent simulation method and numerical implementation technology of crack propagation in rock mass. Firstly, weak surfaces such as cracks were simulated equivalently by dispersing to adjacent solid elements. Secondly, the stress intensity factor at the crack tip was estimated using the stress extrapolation method in accordance with the fracture propagation principle, and the pattern of fracture propagation was identified. The crack coalescence path was then examined using the maximum circumferential tensile stress criteria and the maximum shear stress criterion under various propagation patterns. Finally, the dynamic propagation and coalescence evolution of cracks were realized by crack propagation and intersection treatments. The rationality of the proposed method was verified by uniaxial compression of typical rock specimens with double cracks. Based on the multi-level cutting slope with cracked rocks along an expressway, the crack propagation mechanism and the evolution of slope failure path under excavation unloading were studied.

2 Dynamic propagation simulation of multiple cracks based on crack fracture and propagation criterion

2.1 Fracture and propagation criterion of crack

In rock mass engineering such as rock slope engineering, cracks mainly propagate in tensile and shear patterns under complex stress conditions[13]. In the process of crack propagation, the stress state evolves constantly, and the two propagation patterns often transform into each other, for example, tensile crack propagation can be transformed into shear type, or shear crack propagation can be transformed into tensile type. Different crack propagation discriminating methods must be used to determine the various stress levels and related crack propagation types. To judge the crack propagation patterns in a complicated stress environment, Chao and Liu[28] developed a judgment approach that is now often applied in fracture analysis software like Franc[29]. This study used the fracture propagation analysis method proposed by Chao and Liu[28] to carried out dynamic multi-crack propagation simulation analysis.

2.1.1 Initiation and propagation criterion of tensile crack

Maximum hoop stress criterion (MHSC)[30] is used as the tensile crack initiation and propagation criterion. The following equation is used to determine the crack propagation direction θ_t:

$$\theta_t = \arccos\frac{3K_{II}^2 + \sqrt{K_I^4 + 8K_I^2K_{II}^2}}{K_I^2 + 9K_{II}^2} \tag{1}$$

where K_I and K_{II} are the mode I and mode II stress intensity factors.

When tensile propagation happens, the stress intensity factors at crack tip K_I and K_{II} satisfy the envelope:

$$K_I\cos^3\frac{\theta_t}{2} - \frac{3}{2}K_{II}\sin\theta_t\cos\frac{\theta_t}{2} = K_{IC} \tag{2}$$

where K_{IC} is the fracture toughness of the material in a pure tensile state.

2.1.2 Initiation and propagation criterion of shear crack

Maximum shear stress criteria (MSSC) is used as the shear initiation and propagation criterion of crack. The non-closed (fitting) solution for crack initiation angle of shear propagation is as follows

$$\theta_s = 9.347\times10^{-7}D^4 - 3.222\times10^{-5}D^3 + 9.086\times10^{-4}D^2 + 0.287D - 0.049 \tag{3}$$

where $D = \tan^{-1}(K_I / K_{II})$.

When shear propagation occurs, the stress intensity factors at crack tip K_I and K_{II} satisfy the envelope:

$$\frac{\sigma_C}{2\tau_C}\cos\frac{\theta_s}{2}\left[K_I\sin\theta_s + K_{II}(3\cos\theta_s - 1)\right] = K_{IC} \tag{4}$$

where σ_C and τ_C are the critical tensile stress and critical shear stress of materials, and the values of τ_C / σ_C range from 0.5 to 1.0, corresponding to different types of materials from ductile materials to brittle materials[28]. The ductility of different rock materials is different, and rock failure patterns are closely related to the material ductility[31]. Because the ductility of most rocks is between brittleness ($\tau_C / \sigma_C = 1.0$) and ductility ($\tau_C / \sigma_C = 0.5$), $\tau_C / \sigma_C = 0.7$ is determined as a compromise.

2.1.3 Crack propagation pattern identification

The method proposed by Chao and Liu[28] was adopted to distinguish the crack propagation type under composite stress state, specifically, the envelopes of tensile propagation (Eq. (2)) and shear propagation (Eq. (4)) are drawn in the K_I–K_{II} coordinate system at the same time, and the crack initiation and propagation types are identified according to the distribution position of the stress state at the crack tip in this coordinate system, as shown in Fig. 1. The point T is the intersection of the envelopes of MHSC and MSSC, and the line OT is the dividing line between tensile and shear propagation, with a slope expressed as

$$\frac{K_{II}}{K_I} = \frac{3\cos\frac{\theta_t}{2}\sin\theta_t + \frac{\sigma_C}{\tau_C}\cos\frac{\theta_s}{2}(3\cos\theta_s - 1)}{2\cos^3\frac{\theta_t}{2} - \frac{\sigma_C}{\tau_C}\cos\frac{\theta_s}{2}\sin\theta_s} \tag{5}$$

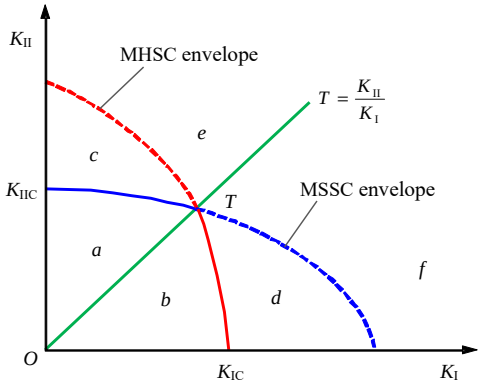

Fig. 1 Discrimination of crack propagation in tensile or shear pattern[28]

The envelopes of MHSC and MSSC and the straight line OT divide the coordinate system into six regions, and each region corresponds to different crack propagation conditions. When the stress states at the crack tip are in regions *a* and *b*, the crack propagation does not occur. When the stress states at the crack tip are in the region *c*, shear propagation occurs at the crack tip. When the stress state at the crack tip is in the region *d*, the tensile propagation at the crack tip occurs. When the stress state at the crack tip is in regions *e* and *f*, both tensile propagation and shear propagation at the crack tip can occur. The region *e* is dominated by tensile propagation, while the

region *f* is dominated by shear propagation.

2.2 Simulation flow of dynamic crack propagation

Based on the crack propagation analysis method described in Section 2.1 and continuous numerical simulation methods such as conventional finite element method and finite difference method, a simulation method for dynamic crack propagation under the action of multiple cracks (crack network) was proposed. The flow of this proposed simulation method is shown in Fig. 2. Compared with conventional continuous medium simulation methods, the crack propagation calculation is added in the proposed method, and the proposed method includes the steps of stress intensity factor calculation, crack initiation judgment, crack initiation angle calculation, crack propagation distance determination, and new crack propagation segment generation.

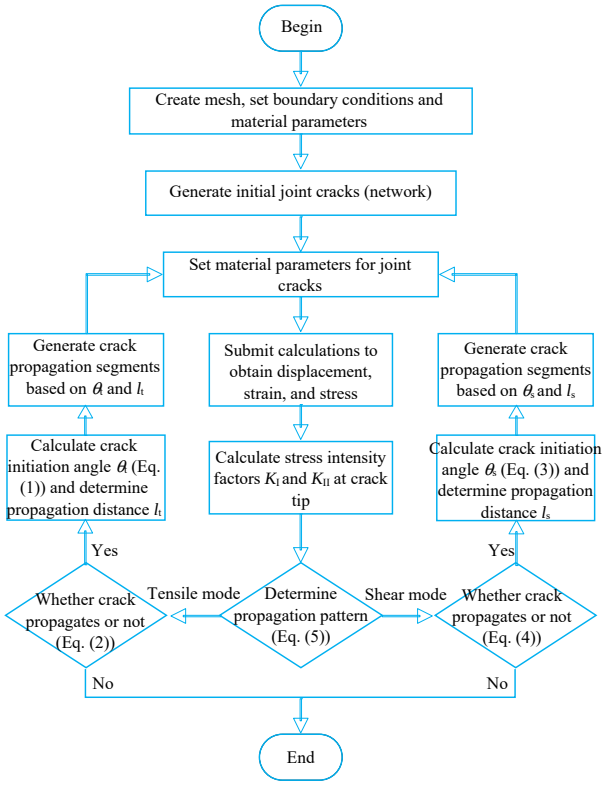

Fig. 2 Simulation flow of dynamic crack propagation

(1) Equivalent simulation of crack. Based on the traditional numerical simulation methods for continuous media, the local solid element weakening method is adopted to equivalently simulate the crack (Section 2.3.1), which is the basis of dynamic crack propagation simulation.

(2) Stress intensity factor calculation and propagation type judgment. The mode I and mode II stress intensity factors K_{I} and K_{II} at the crack tips are calculated by stress extrapolation method (Section 2.3.2), and the propagation type is judged by Eq. (5) based on the calculated stress intensity factors.

(3) Judgment of crack initiation. According to the propagation type, Eqs. (2) and (4) are used to judge whether tensile or shear crack initiation and propagation occurs at the crack tips.

(4) Crack propagation calculation. After judging that the crack initiation can occur at the crack tips at the previous step, the crack initiation angle θ is calculated by Eq. (1) or Eq. (3), and the propagation distance l at this step is determined (Section 2.3.1).

(5) Generation of crack propagation segment. According to the calculated crack initiation angle θ and the determined propagation distance l, a new crack propagation segment is generated, and the values are assigned to the material parameters in the generated segment. When the crack intersects with the existing crack in the process of dynamic crack propagation, the treatment method is given in Section 2.3.3.

2.3 Simulation technology of dynamic crack propagation

2.3.1 Equivalent simulation of crack

The method of weakening local solid elements is used to create initial cracks and simulate crack propagation equivalently, as shown in Fig. 3, and the equivalent simulation method of crack is similar to the equivalent description method of crack in references [27, 32−35]. The specific simulation processes are as follows:

(1) Determination of the spatial position of the initial crack (network) (Fig. 3(a)). For example, the spatial position can be determined by one endpoint of a crack plus dip angle and length of the crack, or by two endpoint positions of the crack.

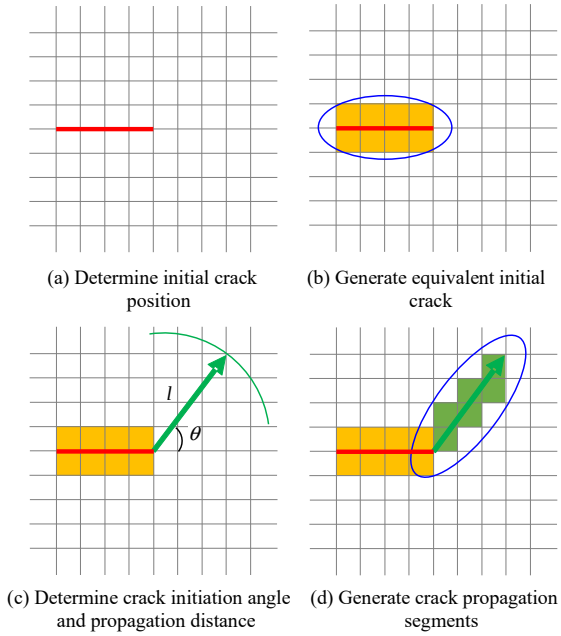

(a) Determine initial crack position (b) Generate equivalent initial crack

(c) Determine crack initiation angle and propagation distance (d) Generate crack propagation segments

Fig. 3 Equivalent simulation and dynamic propagation of cracks

(2) According to the spatial distribution of cracks, the

solid elements through or adjacent to which cracks go are grouped and numbered, and their material strength and stiffness are weakened, so as to form equivalent initial cracks (Fig. 3(b)).

(3) The equivalent simulation of crack in its propagation process is similar to the initial crack generation method. First, the crack initiation angle and propagation distance are obtained (Fig. 3(c)), so as to determine the distribution position of crack tip propagation segment. Then, the solid elements through or adjacent to which cracks pass are grouped and numbered. Finally, a new crack propagation segment is generated by weakening material parameters and thus the crack tip position is updated (Fig. 3(d)).

The equivalent crack in Fig. 3 is essentially a solid element strip with relatively low strength and stiffness, which is formed by dispersing to adjacent solid elements according to the distribution position of cracks. The crack dispersion rule adopted in present study is as follows. If the crack is located on the interface of solid elements (Fig. 3(a)), at least one solid element at both sides of the crack is dispersed to, thus forming an equivalent crack with a width of at least two solid elements (Fig. 3(b)). If the crack directly passes through or partially passes through the solid element (Fig. 3(c)), at least the solid element through which the crack passes is set as an equivalent crack element (Fig. 3(d)). In addition, the solid elements within a certain range on both sides of the crack can be set as equivalent crack elements according to the actual width of the crack.

The width of equivalent crack is closely related to the element size. Because the crack width has an important influence on the mechanical properties of rock mass and crack, it is particularly important to determine the appropriate element size for the simulation analysis of crack propagation. When the crack width is fixed, the smaller the element size, the more elements on the cross section of crack, the smoother the crack boundary, and the better the crack simulation effect. However, the reduction of element size will lead to the increase of the number of elements in the whole calculation model, which will affect the calculation efficiency. As shown in Fig. 3, to make the equivalent crack boundary continuous, the crack width should be at least twice the size of the element, so the maximum size of the element is

$$(S_e)_{max}=\frac{L_c}{2} \tag{6}$$

However, when the crack width is narrow, the element size in the calculation model must be set to a smaller size due to the limitation of the crack width, which leads to an increase in the number of elements in the calculation model and affects the calculation efficiency. This problem is rarely mentioned in previous studies[27, 32−35]. Under the condition of keeping the overall stiffness of cracks unchanged, the crack width should be appropriately expanded equivalently, so as to balance the simulation accuracy of crack propagation and the calculation efficiency of the model, as shown in Fig. 4.

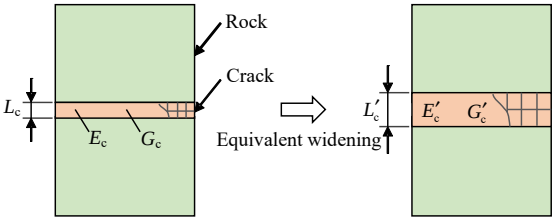

Fig. 4 Equivalent treatment of crack width

If the stiffness (normal stiffness K_n, tangential stiffness K_s) of the crack is not changed before and after the crack width is enlarged, the following requirements must be met

$$\left.\begin{aligned} K_n&=\frac{E_c}{L_c}=\frac{E'_c}{L'_c}\\ K_s&=\frac{G_c}{L_c}=\frac{G'_c}{L'_c}\end{aligned}\right\} \tag{7}$$

where L_c and L'_c are the crack widths before and after the equivalent expansion of crack width; E_c and E'_c are the compressive moduli before and after the equivalent expansion of crack width; and G_c and G'_c are the shear moduli before and after the equivalent expansion of fracture width. If the crack width is enlarged from L_c to L'_c, that is, the element size is enlarged from $(L_c/2)$ to $(L'_c/2)$, the compressive modulus and shear modulus of the crack should be increased to

$$\left.\begin{aligned} E'_c&=\frac{E_cL'_c}{L_c}\\ G'_c&=\frac{G_cL'_c}{L_c}\end{aligned}\right\} \tag{8}$$

2.3.2 Calculation of crack propagation factor

The stress intensity factor at the crack tip calculated by extrapolation method is used as the crack propagation factor. Because of the singularity of crack tip stress in linear elastic materials, the material stiffness degradation at the crack tip is usually used to eliminate this singularity in numerical calculation[36]. However, this method of eliminating stress singularity brings a large error to the stress calculation at the crack tip. As a result, the stress intensity factor at the crack tip cannot be calculated directly by the stress of the crack tip element. Among the numerical methods for stress intensity factor calculation, the extrapolation method is a simple and direct method, including the extrapolation method based on element stress and

the extrapolation method based on crack tip opening displacement. The extrapolation method based on element stress is used to calculate the stress intensity factor, and its calculation principle is shown in Fig. 5.

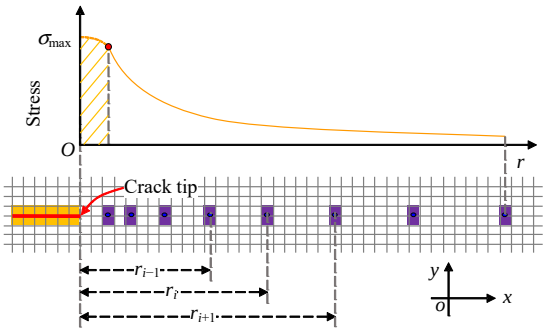

Fig. 5 Stress distribution at crack tip and calculating point selection in stress-extrapolation method

In the stress extrapolation method, the stress intensity factors near the crack tip are assumed to be linear functions of the distance

$$\left.\begin{aligned}\hat{K}_{\mathrm{I}} &= A_1 r + B_1 \\ \hat{K}_{\mathrm{II}} &= A_2 r + B_2\end{aligned}\right\} \tag{9}$$

where A_1, A_2, B_1, and B_2 are fitting parameters. When the value of r tends to be zero, the intercepts in Eq. (9) B_1 and B_2 correspond to the mode I and mode II stress intensity factors at the fracture tip. By substituting the distance between the point near the crack tip and the crack tip r_i and its corresponding stress intensity factors $K_{\mathrm{I}i}$ and $K_{\mathrm{II}i}$ into Eq. (9), such as (r_i, $K_{\mathrm{I}i}$) and (r_i, $K_{\mathrm{II}i}$), the stress intensity factors at the crack tip K_{I} and K_{II} can be extrapolated. According to the linear regression method, the expressions of stress intensity factors at the crack tip are as follows:

$$\left.\begin{aligned}K_{\mathrm{I}} &= \frac{\sum r_i \sum r_i \sigma_{yi}\sqrt{2\pi r_i} - \sum r_i^2 \sum \sigma_{yi}\sqrt{2\pi r_i}}{\left(\sum r_i\right)^2 - N\sum r_i^2} \\ K_{\mathrm{II}} &= \frac{\sum r_i \sum r_i \tau_{xyi}\sqrt{2\pi r_i} - \sum r_i^2 \sum \tau_{xyi}\sqrt{2\pi r_i}}{\left(\sum r_i\right)^2 - N\sum r_i^2}\end{aligned}\right\} \tag{10}$$

We take a rock plate with a crack at the center as an example to demonstrate the calculation method of stress intensity factor at the crack tip and its considerations, as shown in Fig. 6. The geometrical dimensions of the plate (Fig. 6(a)) are: half width W is 100 mm, half height H is 200 mm, plate thickness is 1 mm, half crack length a is 20 mm, and crack width b is 1 mm. The uniform stress acting on both ends of the cracked plate is 10 MPa. The elastic modulus E of the material is 20 GPa and Poisson's ratio ν is 0.25. The method shown in Fig. 3 is used to simulate cracks equivalently, and the calculation results are shown in Fig. 6(b).

The stress distribution at the crack tip is shown in Fig. 6(c). The distribution of stress intensity factors near the crack tip calculated by the stress distribution in Fig. 6(c) is presented in Fig. 6(d) and the stress intensity factors at the crack tip obtained by extrapolation using different value points are presented in Fig. 6(e). Due to the poor regularity of stress distribution at the crack tip (Fig. 6(c)), the reliability of stress intensity factor extrapolated from the first point of the crack tip is low (Fig. 6(d)), while the reliability of stress intensity factor extrapolated after ignoring the first two or three points of the crack tip is high (Fig. 6(e)), which can meet the requirements of crack

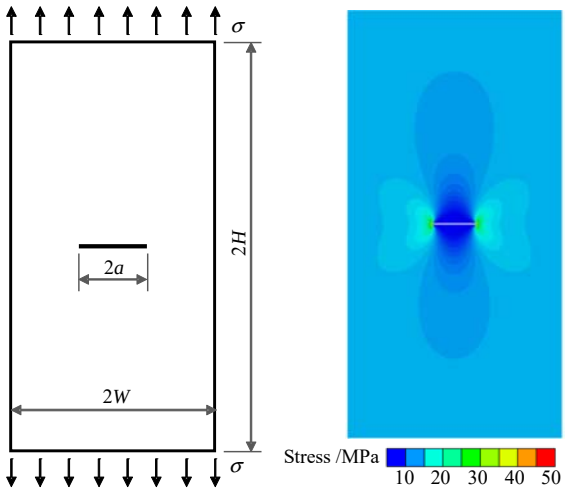

(a) Model diagram (b) Vertical stress

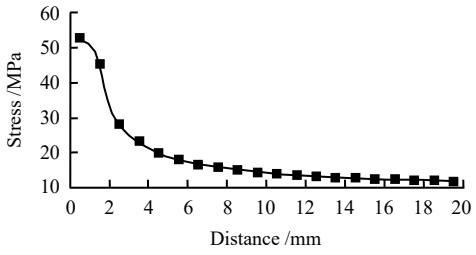

(c) Stress distribution at crack tip

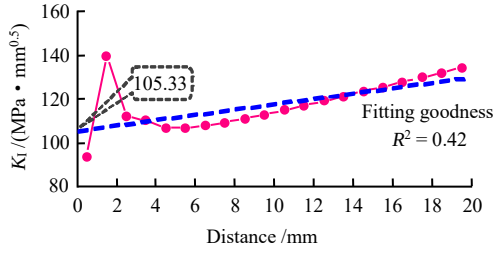

(d) Calculation of stress intensity factor before optimization of value points

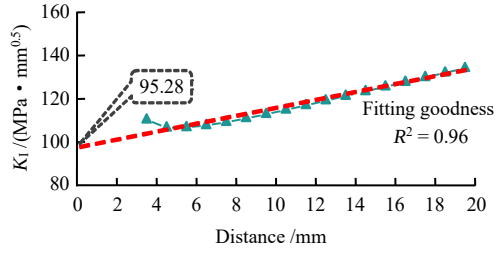

(e) Calculation of stress intensity factor after optimization of value points

Fig. 6 Stress-extrapolation method verification for stress intensity factor calculation of equivalent crack

propagation analysis. It is therefore necessary to neglect the first 2 or 3 points of the crack tips when calculating the stress intensity factor of the crack tip using the equivalent crack simulation and stress extrapolation method proposed in this paper.

2.3.3 Coalescence treatment of crack

The treatment of crack coalescence is a difficult problem in the crack propagation simulation in multi-cracked rock mass. In the crack propagation simulation methods based on fracture mechanics, such as extended finite element and field-enriched finite element, the crack coalescence is usually divided into the coalescence of crack tips, the coalescence of crack tip and crack segment, and the coalescence of crack tip and free boundary[5, 37]. The present study develop a simple crack coalescence treatment method according to the characteristics of equivalent crack propagation simulation, as shown in Fig. 7.

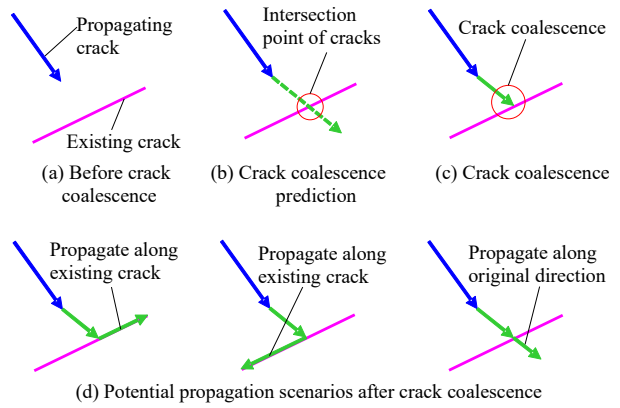

Fig. 7 Treatment method of crack coalescence

Before cracks coalesce, there is a certain distance between a propagating crack and an existing crack, as shown in Fig. 7(a). When the tip of the propagating crack is close to the existing crack, it is judged by calculation whether the propagating crack will meet the existing crack in the next propagation calculation. If the propagating crack will meet the existing crack in the next propagation calculation, the position of the coalescence point is determined (Fig. 7(b)), and the tip of the propagating crack is extended to the coalescence point to complete the coalescence calculation of the cracks (Fig. 7(c)). The tip of the propagating crack is adjusted after the crack coalescence. There are many potential propagating directions of the crack after the crack coalescence: propagating along either end of the existing crack or along the original direction of the propagating crack (Fig. 7(d)). The most probable propagation direction is selected from the potential propagation directions as the propagation direction after the crack coalescence. The judgment method for propagation direction is to calculate the stress intensity factors at the crack tip along different directions and the corresponding distances from the envelope shown in Fig. 1, and the propagation direction of crack is along the direction with the largest distance beyond the envelope. In addition, when the propagating crack meets the coalescence point of the existing crack, the method for judging the next propagation of the crack is similar to that shown in Fig. 7(d), that is, the most likely propagation direction is selected from a plurality of potential propagation directions passing through the coalescence point as the propagation direction.

2.4 Verification of dynamic multi-crack propagation

Two typical rock specimens with double cracks in reference [38] were selected for uniaxial compression simulation, and the rationality and applicability of the proposed method were verified by comparing the simulation results shown in Fig. 8 with the exiting results. The elastic modulus of the rock specimen is 20 GPa, the Poisson's ratio is 0.25, and the mode I fracture toughness is 2.0 MPa·m$^{0.5}$. There is no interaction on the interface under tension, but the friction force on the interface of the crack under compression-shear condition exists. Therefore, the Mohr-Coulomb model was adopted to simulate the mechanical performance of the crack. Both the cohesion and tensile strength are 0, and the internal friction angle is 30°. The strength model and corresponding parameters can ensure the tensile yield of the crack in tensile state and the shear yield when shear stress exceeds shear strength of the crack in compressive-shear state, so that tensile and slip deformations of crack interfaces can be simulated through the plastic flow of crack element. The vertical load on the specimen starts from 0 at a rate of 0.1 MPa per step. The increase of the load is suspended until the crack initiation, and the crack propagation calculation begins.

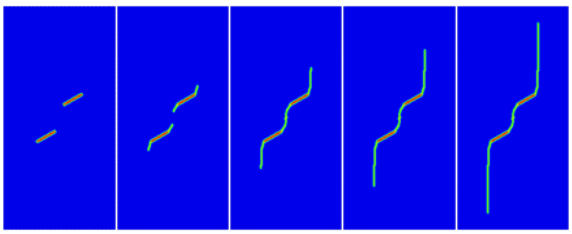

(a) Propagation pattern of double cracks I

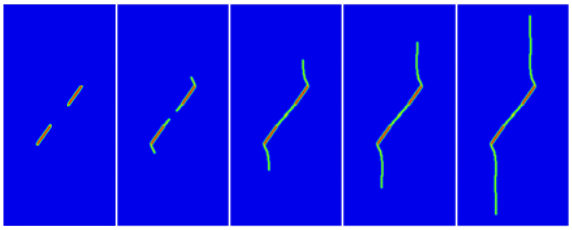

(b) Propagation pattern of double cracks II

Fig. 8 Uniaxial compression simulation of typical double-cracked rock specimens

The dynamic crack propagation processes are displayed in Fig. 8. The final crack propagation path calculated in

Fig. 8 is in good agreement with the experimental results in reference[38], thus demonstrating the rationality of the proposed equivalent simulation method of crack propagation in the analysis of crack propagation path.

The stress intensity factor at the crack tip before crack propagation is extracted and put into the envelope diagram to analyze the crack propagation pattern, as shown in Fig. 9. During uniaxial loading, the stress states at points *A*, *B*, and *D* of the crack tip evolve along paths ①, ②, and ④ in K_{I}–K_{II} coordinate system, and finally reach MHSC envelope and expand in tensile pattern. However, the stress state at point *C* of the crack tip evolves along path ③ in K_{I}–K_{II} coordinate system, and finally reaches the MSSC envelope and develops in shear pattern. The calculated crack propagation patterns are the same as those of uniaxial compression test for specimens with double cracks in reference [38], that is, tensile propagation occurs at points *A*, *B*, and *D* of the crack tip, and shear propagation occurs at point *C* of the crack tip, thus demonstrating the rationality of the proposed crack propagation simulation method in crack propagation pattern analysis.

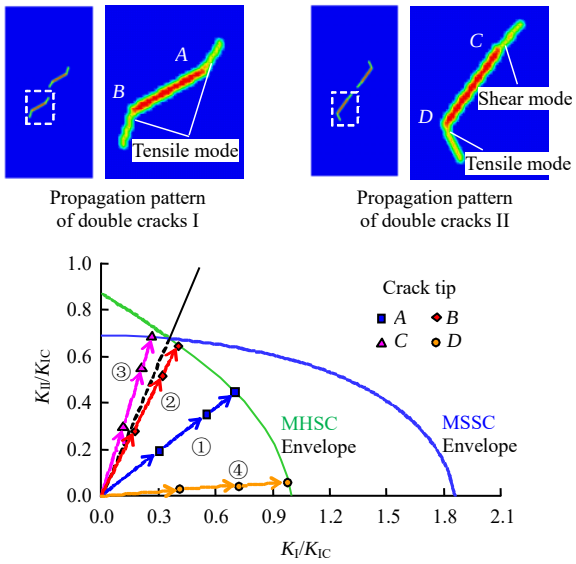

Fig. 9 Stress intensity factor evolution and propagation pattern identification at crack tips

3 Failure path analysis of cracked rock slope under multi-stage excavation unloading

3.1 Overview of engineering project

The proposed simulation method was used to analyze the failure path of a highway cutting slope under multi-stage excavation unloading. The shape and excavation design of the slope are displayed in Fig. 10(a). The slope is in denudation low mountain region and has a natural transverse slope of about 25°. The surface layer of the slope is brown-yellow hard plastic silty clay with a thickness of 1.0−2.0 m, and the underlying strata is strongly to moderately weathered brown-yellow siltstone of the middle Triassic, with medium-thick layered structure and developed cracks, which belongs to soft rock. The excavation profile of the slope is step-shaped, with a slope ratio of 1:1.25, and a bench height of 10 m, as shown in Fig. 10(b).

According to the preliminary geological survey and excavation exposure, two groups of predominant discontinuities are developed in the overlying strata of the slope, and they are gently inclined crack group J1, 320°/SW∠53° and steeply inclined crack group J2, 53°/NW∠87°. Based on the main occurrence characteristics (dip direction and angle) of the cracks in the overlying strata of the slope, the predominant cracks (ignoring the minor cracks with short trace length) of the two groups of dominant cracks are randomly generated, with trace lengths of 3−8 m and spacings of 4−6 m, and the spatial characteristic distribution of cracks is given in Fig. 10(b).

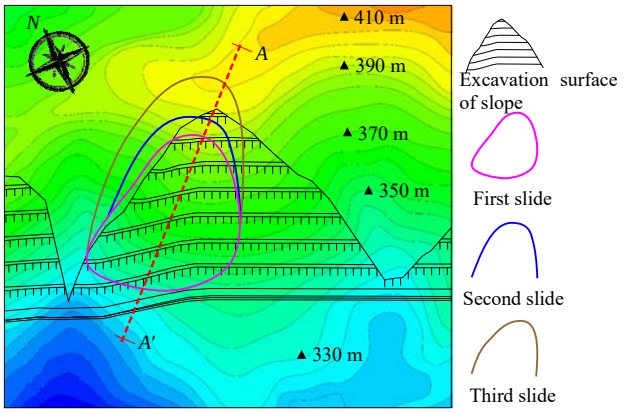

(a) Slope terrain and its excavation and failure regions

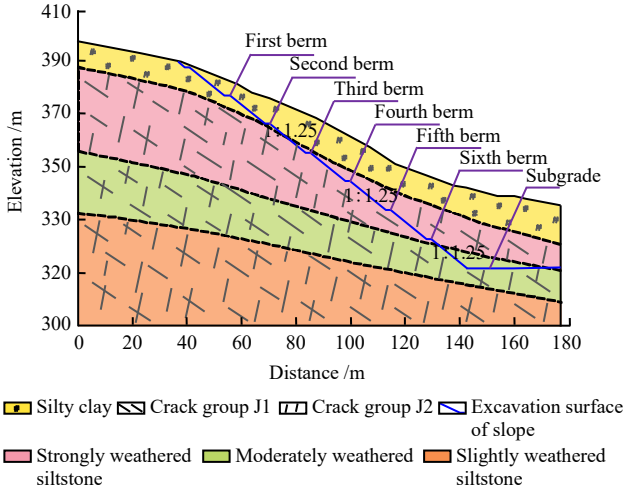

(b) Stratigraphic distribution of *A*-*A*′ slope profile

Fig. 10 General engineering geology of slope

When the slope was excavated to the designed slope toe in January 2022, it slipped many times due to excavation unloading, and the sliding failure status is presented in Fig. 11. Through geological investigation, the failure characteristics of the slope were as follows: tensile cracks

with a width of about 20 cm appeared at the slope top; shear dislocation with a distance of about 30 cm occurred on the slope surface, which was approximately perpendicular to the slope surface and outward; shear displacement of about 20 cm occurred at the slope toe. According to the exposed crack surface characteristics after the sliding failure, the propagation and failure of the tensile cracks at the slope top and the shear cracks at the slope flank and toe were all along the existing cracks. Further combined with the results of geological exploration and deep displacement monitoring at the early stage (Section 3.4), the sliding zones of the slope sliding for many times were speculated to be distributed in cracked rock strata.

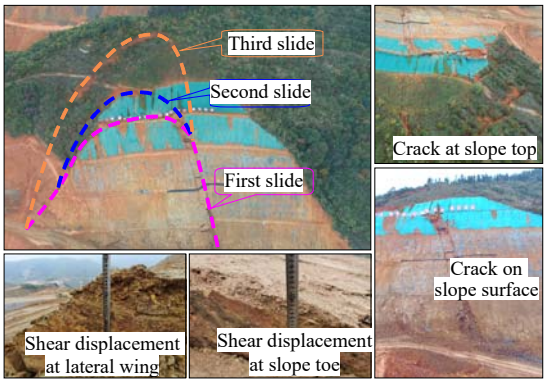

Fig. 11 Geological survey for slope failure characteristics

3.2 Numerical analysis conditions

To clarify the propagation and coalescence of existing cracks and failure characteristics of the slope under excavation unloading, the failure mechanism of the slope under excavation unloading were investigated based on crack propagation. The mechanical parameters of different slope strata were determined through geological survey report and laboratory tests, as shown in Table 1.

Table 1 Geotechnical mechanical parameters of slope

Formation type	Density /(g • cm^{-3})	Cohesion /MPa	Internal friction angle /(°)	Deformation modulus /GPa	Poisson's ratio
Silty clay	1.6	0.042	31	0.5	0.30
Strongly weathered siltstone	2.2	0.350	33	2.0	0.28
Moderately weathered siltstone	2.4	0.460	36	6.0	0.27
Slightly weathered siltstone	2.5	0.730	37	9.0	0.26

According to the distribution of strata in profile, excavation surface, and cracks in the slope displayed as Fig. 10(b), a numerical analysis model of the slope excavation was established, as shown in Fig. 12. The element size of the slope is 0.1 m, and the average width of equivalent crack is 0.2 m. There are 121 cracks in the overlying strata, including 54 cracks with gentle dip angles (group J1) and 67 cracks with steep dip angles (group J2). The crack propagation is simulated using the methods described in Sections 2.1−2.3, and the propagation length of cracks is set to 10 unit lengths (1 m) at a time.

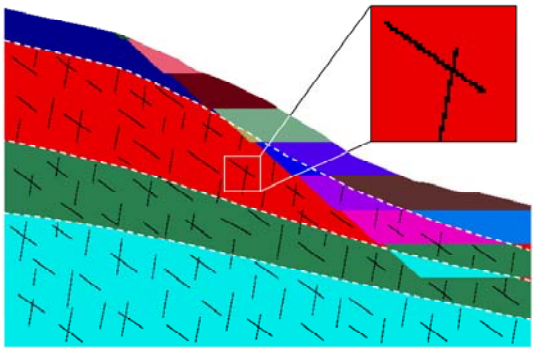

Fig. 12 Numerical calculation model of slope

The linear elastic model was adopted to simulate the complete rock in the overlying strata of the slope, and the stiffness parameters of the model materials were selected from Table 1. According to the rock mechanics parameters shown in Table 1, the shear strength parameters of the slope were converted into fracture toughness by using the conversion method between shear strength parameters and fracture parameters in reference [39]. The mode I fracture toughness of different strata from top to bottom is 0.12, 0.24, 0.45, and 0.56 MPa·m$^{0.5}$. To consider the mechanical properties of crack interfaces under different stress conditions, the parameter setting method for crack material was consistent with that in Section 2.4, and the Mohr-Coulomb model was employed to simulate the crack. The crack strengths of different strata are mainly reflected in the friction coefficients. For the cracks in strongly, moderately, and slightly weathered siltstone, their cohesion and tensile strength were all 0, and their friction coefficients were determined according to the internal friction angles of rocks in the strata, which are 33°, 36°, and 37°.

3.3 Dynamic crack propagation process of slope under excavation unloading

3.3.1 Crack initiation and propagation at bench edge

The crack initiation and propagation processes at bench edge under excavation unloading are shown in Fig. 13, and Fig. 14 shows the distributions of stress intensity factors at points *A*, *B*, and *C* of crack tip during excavation corresponding to Fig. 13.

(a) In the initial state and when the slope is excavated to the first berm, the stress intensity factors of the crack tip at the bench edge are distributed within the envelope, and the crack does not initiate and expand at this time. (b) When the slope is excavated to the second berm, the stress state at point *B* of the crack tip evolves from the inside of the envelope through the MHSC envelope to the outside of the envelope, which indicates that the initiation

and propagation of tensile crack occur at point *B* of the crack tip during this excavation process. (c) When the slope is excavated to the third berm, the initiation and propagation of tensile crack at point *C* of the crack tip are similar to those at point *B*, so the crack initiation and propagation occur at both tips of the crack *BC* at bench edge, forming the dominant propagating cracks.

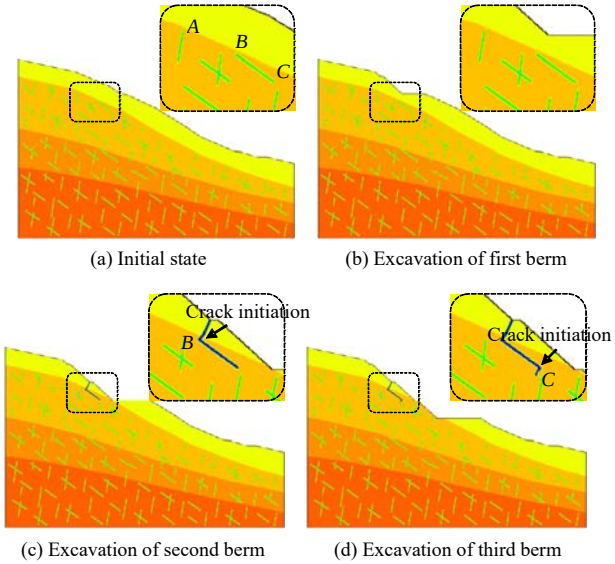

Fig. 13 Upper slope excavation and crack initiation process at bench edge

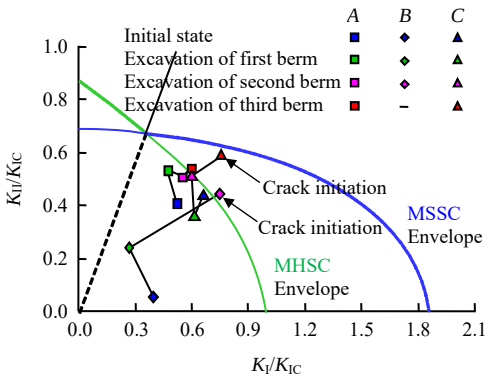

Fig. 14 Upper slope excavation and crack initiation analysis at bench edge

3.3.2 The first sliding failure path

The dominant propagating crack *BC* at the bench edge are taken as the main propagating cracks, and the crack propagation characteristics in the slope during multi-stage excavation are explored, with the calculation results shown in Fig. 15. To analyze the complete failure path of the slope under excavation unloading, whether the crack can initiate during the dynamic crack propagation processes is no longer considered based on the crack initiation analysis in the previous section. Therefore, the failure path calculated in this section is actually the potential (most likely) failure path of the slope under excavation unloading.

(a) The failure surfaces of the slope are composed of the existing cracks in the slope and the fracture surfaces formed by the crack propagation in the rock bridge under excavation unloading. In the middle and upper parts of the slope, the fracture surface mainly expands along the existing cracks with steep and gentle dip angles. While in the lower part of the slope and near the slope toe, the fracture surface mainly expands along the cracks with gentle dip angles, and the cracks with steep dip angles have less influence on the crack propagation path.

(b) The cracks in different parts of the slope or with different dips have different propagation patterns. In the middle and upper parts of the slope, the cracks with gentle dip angles mainly expand in tensile pattern, while the cracks with steep dip angles mainly expand in shear pattern. In the lower part of the slope and near the slope toe, the cracks with gentle dip angles mainly expand in shear pattern, while the cracks with steep dip angles are not easy to expand.

(c) The shape of crack propagation path has obvious spatial distribution characteristics. During downward excavation unloading process of the slope, the crack propagates downward from the bench edge along the slope surface, the step-shaped crack propagation path occurs in the middle and upper parts of the slope, the arc-shaped crack propagation path occurs in the lower part of the slope, and the sliding body finally slides out from the slope toe.

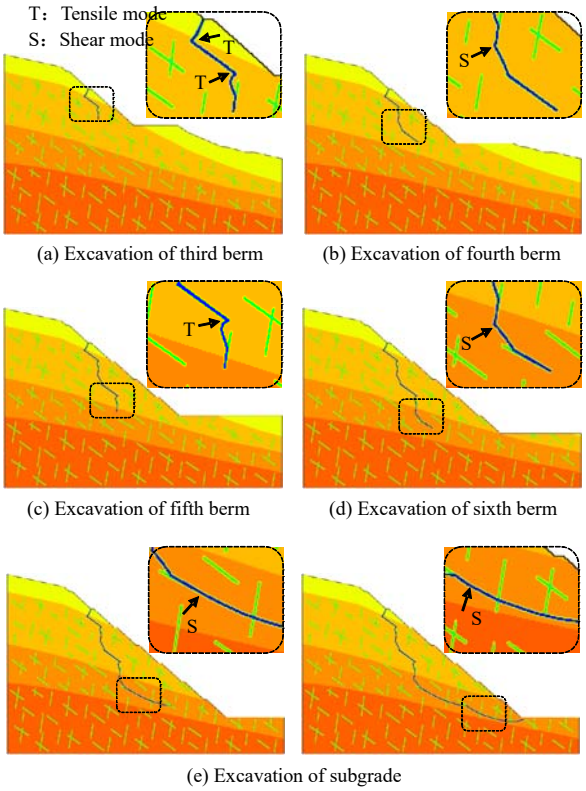

Fig. 15 Crack propagation path during excavation of middle and lower slope parts

3.3.3 The second sliding failure path

The investigation on the second sliding failure path

of the slope is similar to that on the first sliding failure path. It is necessary to judge or specify the initial initiation and propagation position of the crack to form the dominant propagating crack, and then the crack propagation pattern and path are examined based on the dominant crack. According to the evolution law of stress intensity factor of the crack tip at the bench edge during the excavation of the upper part of the slope in Fig. 14, the stress state at point *A* of the crack tip at the bench edge is close to MHSC envelope in K_{I}–K_{II} coordinate system, demonstrating easy initiation and propagation of the crack. Therefore, the point *A* of the crack tip at the bench edge is designated as the crack initiation point of the second sliding failure. Other analysis conditions are consistent with those in the simulation of the first sliding failure path of the slope. The calculation results of the second sliding failure path of the slope are shown in Fig. 16.

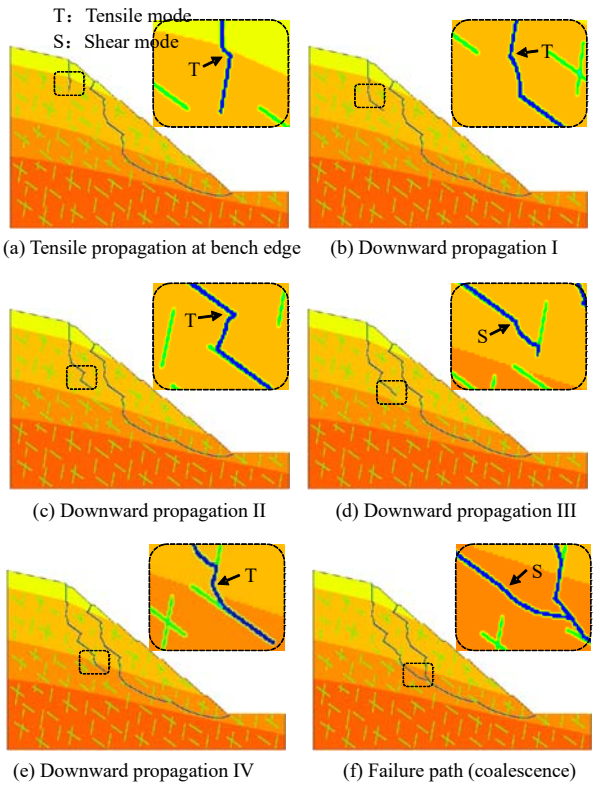

Fig. 16 Crack propagation path of second rockslide

Comparing Fig. 16 with Fig. 15 shows that there are many similarities between the second sliding failure processes and the first sliding failure processes in the development direction of fracture surface and the shape of fracture path. However, the two sliding failure processes of the slope have the following different characteristics:

(a) The crack propagation patterns are different at the same elevation. In the second sliding failure processes, the cracks with steep dip angles in the middle and upper parts of the slope mainly expands in tensile mode, while the cracks with gentle dip angles mainly expands in shear mode. In the first sliding failure processes, the cracks with steep dip angles in the middle and upper parts of the slope expand in shear mode, while the cracks with gentle dip angles expand in tensile mode.

(b) The spatial distribution characteristics of crack propagation paths are different. The first sliding failure surface of the slope extends downward from the bench edge and slides out from the slope toe. However, the second sliding failure surface mainly occurs in the middle and upper parts of the slope, and the failure surface extends downward from the slope top and then intersects with the first sliding failure surface in the middle part of the slope, thus forming an interconnected failure path.

3.3.4 Deformation distribution law

The deformation distributions of the slope when the failure paths are interconnected are presented in Fig. 17.

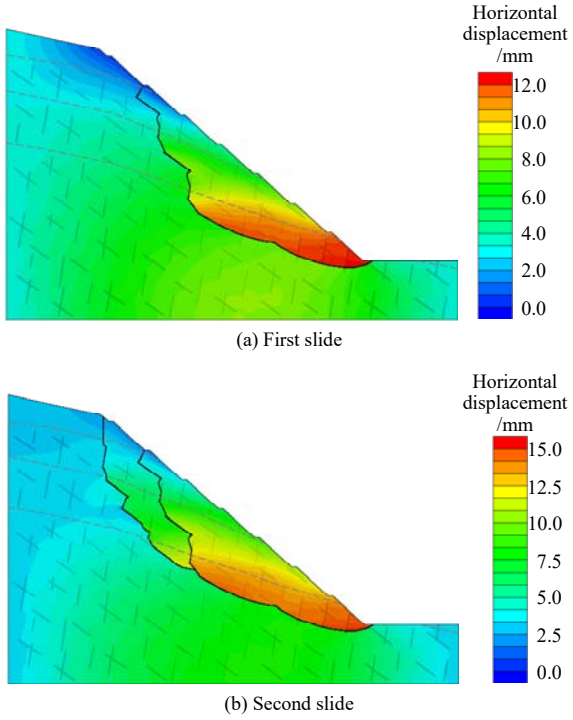

Fig. 17 Sliding deformation distribution of rockslide

(a) After the first failure surface of the slope is interconnected, the whole sliding body slides towards the slope surface, and the sliding deformation of the lower part of the sliding body (the maximum deformation is about 13 mm) is significantly higher than that of the upper part of the sliding body (the minimum deformation is about 1 mm), as shown in Fig. 17(a).

(b) After the second failure surface of the slope is interconnected, the newly generated sliding body slides to the slope surface, and the deformation of the sliding body presents the distribution characteristics of small at upper part (the minimum deformation is about 2 mm) and large at lower part (the maximum deformation is about 11 mm), as shown in Fig. 17(b).

(c) The deformation of the second sliding body is less than that of the first sliding body due to the blocking

action of the first sliding body, and the deformation of the first sliding body increases by 2−3 mm due to the pushing action of the second sliding body.

3.4 Comparison between simulation and monitoring data of crack propagation

The comparison between the abovementioned numerical results and the monitored deep deformation distributions before and after slope failure (Figs 18(a) and 18(b)), as well as the estimated sliding failure range based on monitoring data and site investigation on the landslide (Fig. 18(c)), are shown in Fig. 18. On January 2, 2022, the installations of the inclinometer with a length of 30 m at the third berm and the inclinometer with a length of 20 m at the fifth berm were completed (the installation positions are given in Fig. 18(c)), and the deep horizontal deformation monitoring of the slope began. On January 4, 2022, the landslide occurred, and the inclinometer was damaged due to excessive local deformation. The monitoring data before the damage of the inclinometer are shown in Figs. 18(a) and 18(b). The monitoring data from the inclinometer with a length of 30 m at the third berm show that the maximum horizontal deformation in the deep slope part is around 18 mm during the monitoring period, and the sliding failure position occurs within the depth range of 25−28 m the third berm downward, as shown in Fig. 18(a). The monitoring data from the inclinometer with a length of 20 m at the fifth berm show that the maximum horizontal deformation in the deep slope part is about 14 mm during the monitoring period, and the sliding failure position occurs within the depth range of 16−18 m the fifth berm downward, as shown in Fig. 18(b).

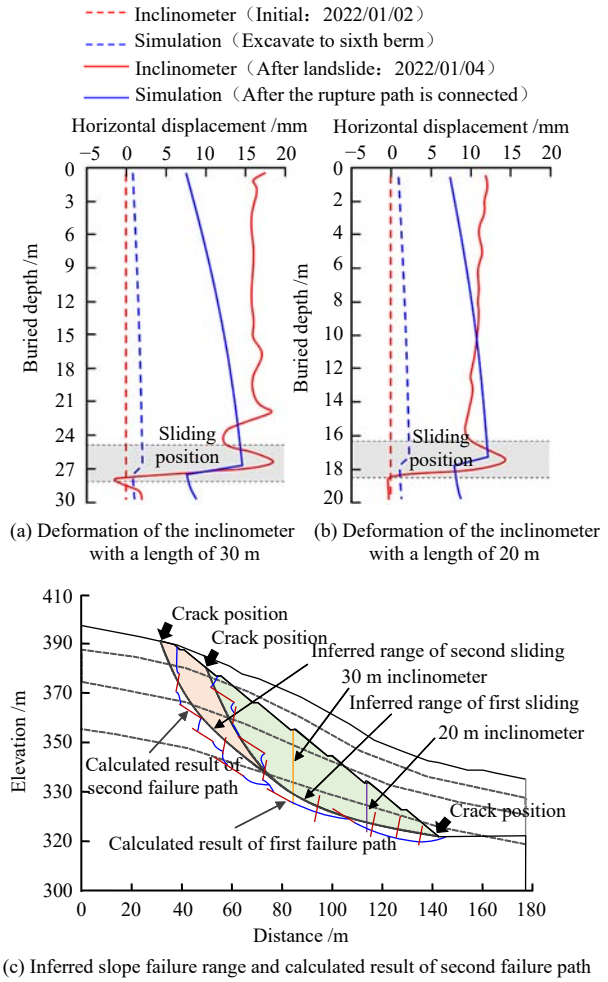

(a) Deformation of the inclinometer with a length of 30 m (b) Deformation of the inclinometer with a length of 20 m

(c) Inferred slope failure range and calculated result of second failure path

Fig. 18 Comparison of monitored/investigated results and calculated results of rockslide

The calculated horizontal deformations of the slope when the first sliding failure surface is interconnected are compared with the monitoring data, as shown in Figs. 18(a) and 18(b). The calculated horizontal deformations of the slope are relatively smaller compared with the monitoring results, but the calculated deformation distribution trends and sliding band positions have high similarity with the monitoring results.

Combining the monitoring results of deep slope displacement with the geological survey results such as the landslide crack distribution, the sliding failure range of the slope can be inferred, as shown in Fig. 18(c). The calculated failure path distribution is compared with the predicted slope sliding failure range, it is found that the numerical results of the slope failure path are in good agreement with the two predicted slope sliding failure ranges in the overall trend, which shows that the failure path analysis of the slope under excavation unloading based on crack propagation is reasonable.

3.5 Discussion on failure pattern of cracked rock slope under excavation unloading

The failure pattern and path of cracked rock slope has been a hot issue in slope engineering field. For example, Huang et al.[3], Scholtès and Donze[11], and Zhu et al.[13] used the strength reduction method to simulate the failure pattern of natural cracked rock slope by particle discrete element method, and Chen et al.[20], Zhou[21], and Aliha et al.[26] studied the fracture path of typical cracked rock slope based on fracture mechanics judgment. Compared with the existing research, the characteristic of this paper is that the crack propagation criterion under complex stress environment is developed into numerical simulation, and the influence of excavation unloading on crack initiation and propagation is analyzed from the mechanical point of view of crack propagation. Furthermore, the crack distribution (crack network) considered in this paper is more complex and more suitable for engineering practice.

Further analysis of the above numerical results shows that the crack initiation and propagation mechanism and failure path distribution law of cracked rock slope under excavation unloading are as follows:

(1) The crack initiation and propagation of the slope begins from the crack tip at the bench edge. As the excavation unloading of the upper part of the multi-stage slope advances, the stress state of the crack at the bench edge is adjusted, and the stress intensity factor at the crack

tip gradually approaches and exceeds the MHSC envelope, which leads to the initiation and propagation of tensile crack at the bench edge and form the dominant propagating crack under excavation unloading.

(2) The tensile-shear mixed propagation of crack occurs in the middle and upper parts of the slope, and the propagation path is step-shaped. In the middle and upper parts of the slope, the propagation pattern of crack is significantly affected by the crack distribution (crack network) and the dip angle of crack. For example, in the upper part of the first sliding failure surface near the slope surface, the propagation of cracks with gentle and steep dip angles are mainly tensile and shear modes, while in the second sliding failure surface near the deep slope, the propagation modes of cracks with gentle and steep dip angles are opposite to those near the slope surface due to the change of stress environment. The fracture surface formed by the crack propagation in the middle and upper parts of the slope intersects with the existing cracks and expands along the tip of the intersected cracks, thus forming a step-shaped propagation path.

(3) The shear propagation occurs in the lower part of the slope and near the slope toe, and the propagation path is arc-shaped. Because of the obvious shear action in the lower part of the slope and near the slope toe, the propagation of the crack in this part is mainly in shear mode, and the propagation path is mainly controlled by the distribution form of the maximum shear stress at the slope toe, which is approximately arc-shaped. At the slope toe, the crack with gently dip angle has a certain influence on the propagation path because its trace is consistent with the direction of the maximum shear stress gradient, while the crack with steep dip angle has less influence on the propagation path because its trace is approximately perpendicular to the direction of the maximum shear stress gradient.

The third landslide happened after the first two landslides. Authors deemed that the 3rd landslide was similar to the 2nd landslide in terms of mechanism of occurrence through the geological findings of the 3rd landslide such as fracture distribution, slide surface characteristics, and slide range, and so no discussion was made. In addition, because excavation unloading is the condition that leads to crack propagation along the slope, the judgment of crack initiation primarily takes into account the crack at the bench edge that is first affected by the excavation unloading process. However, this judgment has some restrictions on the selection range of potential initial crack initiation, necessitating further optimization of the judgment of crack initiation.

4 Conclusions

The crack propagation criterion under complex stress conditions was developed into numerical simulation, and the crack propagation mechanism and the failure path development law of the slope under multi-stage excavation unloading were simulated and analyzed from the perspective of crack propagation. The main conclusions are drawn as follows:

(1) The crack network was equivalently simulated by weakening local solid elements, and the dynamic crack propagation simulation with complex crack network was accomplished by integrating stress intensity factor calculation, crack propagation pattern recognition, and crack coalescence treatment techniques. The rationality of the proposed method in simulating crack initiation and propagation was verified by uniaxial compression of typical rock samples with double cracks, and its applicability in rock slope failure analysis was verified by numerical analysis on failure path of the slope under excavation unloading.

(2) Under multi-stage excavation unloading from top to bottom, the stress state at the bench edge evolves continuously, and the tensile crack initiation and propagation at the bench edge first occurs. As the slope excavation advances, the crack at the bench edge propagate downward along the slope surface and form the predominant propagating crack during excavation unloading.

(3) The tensile-shear mixed crack propagation occurs in the middle and upper parts of the slope, and cracks with various dip angles and locations propagate in diverse patterns. The crack surface in the middle and upper parts of the slope is formed by the coalescence of existing cracks and the fracture surface formed by crack propagation, and the failure propagation path is step-shaped.

(4) The crack propagates in shear pattern in the lower part of the slope and at the slope toe, and the arched propagation path is mostly governed by the maximum shear stress distribution at the slope toe. The crack with a gentle dip angle has certain influence on the propagation path, while the crack with a steep dip angle has less influence.

References

[1] GU Dong-ming, GAO Xue-cheng, ZHANG Wen-gang, et al. Failure evolution of anti-dip rock slope in the Three Gorges reservoir area[J]. Rock and Soil Mechanics, 2020, 41(Suppl.2): 1−10.

[2] CAMONES L A M, VARGAS E D, DE FIGUEIREDO R P, et al. Application of the discrete element method for modeling of rock crack propagation and coalescence in the step-path failure mechanism[J]. Engineering Geology, 2013, 153: 80−94.

[3] HUANG D, CEN D, MA G, et al. Step-path failure of rock slopes with intermittent joints[J]. Landslides, 2015, 12(5): 911−926.

[4] EBERHARDT E, STEAD D, COGGAN J S. Numerical analysis of initiation and progressive failure in natural rock slopes - the 1991 Randa rockslide[J]. International Journal of Rock Mechanics and Mining Sciences, 2004, 41(1): 69−87.

[5] ZHOU X, CHEN J. Extended finite element simulation of step-path brittle failure in rock slopes with non-persistent en-echelon joints[J]. Engineering Geology, 2019, 250: 65−88.

[6] MULLER J R, MARTEL S J. Numerical models of translational landslide rupture surface growth[J]. Pure and Applied Geophysics, 2000, 157(6-8): 1009−1038.

[7] AN X, NING Y, MA G, et al. Modeling progressive failures in rock slopes with non-persistent joints using the numerical manifold method[J]. International Journal for Numerical and Analytical Methods in Geomechanics, 2014, 38(7): 679−701.

[8] WANG C, TANNANT D D, LILLY P A. Numerical analysis of the stability of heavily jointed rock slopes using PFC2D[J]. International Journal of Rock Mechanics and Mining Sciences, 2003, 40(3): 415−424.

[9] LI L C, TANG C A, ZHU W C, et al. Numerical analysis of slope stability based on the gravity increase method[J]. Computers and Geotechnics, 2009, 36(7): 1246−1258.

[10] SCHOLTES L, DONZE F V. Modelling progressive failure in fractured rock masses using a 3D discrete element method[J]. International Journal of Rock Mechanics and Mining Sciences, 2012, 52: 18−30.

[11] SCHOLTES L, DONZE F V. A DEM analysis of step-path failure in jointed rock slopes[J]. Comptes Rendus Mecanique, 2015, 343(2): 155−165.

[12] JIANG M J, JIANG T, CROSTA G B, et al. Modeling failure of jointed rock slope with two main joint sets using a novel DEM bond contact model[J]. Engineering Geology, 2015, 193: 79−96.

[13] ZHU Lei, HUANG Run-qiu, YAN Ming, et al. Step-path failure mechanism of rock slopes based on crack coalescence modes in rock mass[J]. Chinese Journal of Geotechnical Engineering, 2017, 39(7): 1216−1225.

[14] DA SILVA B G, EINSTEIN H H. Modeling of crack initiation, propagation and coalescence in rocks[J]. International Journal of Fracture, 2013, 182(2): 167−186.

[15] CHEN C H, WANG C L. A fracture mechanics stability analysis of a rock slope with a tensile crack[J]. Electronic Journal of Geotechnical Engineering, 2007, 12(C): 1−5.

[16] THARP T M, COFFIN D T. Field application of fracture mechanics analysis to small rock slopes[C]//Proceedings of the 26th US Symposium on Rock Mechanics (USRMS). Rapid City: [s. n.], 1985.

[17] SINGH R, SUN G. Fracture mechanics applied to slope stability analysis[C]//Proceedings of the International Symposium on Surface Mining-Future Concepts. [S. l.]: University of Nottingham, 1989.

[18] SCAVIA C. Fracture-mechanics approach to stability analysis of rock slopes[J]. Engineering Fracture Mechanics, 1990, 35(4-5): 899−910.

[19] KEMENY J. The time-dependent reduction of sliding cohesion due to rock bridges along discontinuities: a fracture mechanics approach[J]. Rock Mechanics and Rock Engineering, 2003, 36(1): 27−38.

[20] CHEN Hong-kai, XIAN Xue-fu, TANG Hong-mei. Stability analysis method for perilous rock by fracture mechanics[J]. Journal of Chongqing University: Natural Science Edition, 2009, 32(4): 434−437, 452.

[21] ZHOU Yun-tao. A method for calculating the stability of unstable rocks on Three Gorges Reservoir by fracture mechanics[J]. Rock and Soil Mechanics, 2016, 37(Suppl.1): 495−499.

[22] GAO W, DAI S, XIAO T, et al. Failure process of rock slopes with cracks based on the fracture mechanics method[J]. Engineering Geology, 2017, 231: 190−199.

[23] CHANG Z, CAI Q, ZHOU W, et al. Effects of the loading and unloading conditions on crack propagation in high composite slope of deep open-pit mine[J]. Advances in Civil Engineering, 2019: 3168481.

[24] ZHOU Z, CHEN Z. Parallel offset crack interactions in rock under unloading conditions[J]. Advances in Materials Science and Engineering, 2019(2019): 1430624.

[25] HAERI H, KHALOO A, MARJI M F. A coupled experimental and numerical simulation of rock slope joints behavior[J]. Arabian Journal of Geosciences, 2015, 8(9): 7297−7308.

[26] ALIHA M M, MOUSAVI M, AYATOLLAHI M. Mixed mode I/II fracture path simulation in a typical jointed rock slope[C]//Proceedings of the 4th International Conference on Crack Paths. Gaeta, Italy: [s. n.], 2012.

[27] ZHANG K, CAO P, MENG J, et al. Modeling the progressive failure of jointed rock slope using fracture mechanics and the strength reduction method[J]. Rock Mechanics and Rock Engineering, 2015, 48(2): 771−785.

[28] CHAO Y J, LIU S. On the failure of cracks under mixed-mode loads[J]. International Journal of Fracture, 1997, 87(3): 201−223.

[29] PETTIT R, ANNIGERI B, OWEN W, et al. Next generation 3D mixed mode fracture propagation theory including HCF–LCF interaction[J]. Engineering Fracture Mechanics, 2013, 102: 1−14.

[30] ERDOGAN F, SIH G. On the crack extension in plates under plane loading and transverse shear[J]. Journal of Basic Engineering, 1963, 85: 519−525.

[31] ERARSLAN N, GHAMGOSAR M. Fracturing and indirect tensile strength of brittle and ductile rocks[C]// Proceedings of the ISRM Regional Symposium- EUROCK 2014. Leiden: [s. n.], 2014.

[32] LIU H L, LI L C, LI S H, et al. The time-dependent failure mechanism of rocks and associated application in slope engineering: an explanation based on numerical investigation[J]. Mathematical Problems in Engineering, 2020(7): 1680265.

[33] KONIETZKY H, HEFTENBERGER A, FEIGE M. Life-time prediction for rocks under static compressive and tensile loads: a new simulation approach[J]. Acta Geotechnica, 2009, 4(1): 73−78.

[34] LI X, KONIETZKY H, LI X. Numerical study on time dependent and time independent fracturing processes for brittle rocks[J]. Engineering Fracture Mechanics, 2016, 163: 89−107.

[35] FU J, ZHANG X, ZHU W, et al. Simulating progressive failure in brittle jointed rock masses using a modified elastic-brittle model and the application[J]. Engineering Fracture Mechanics, 2017, 178: 212−230.

[36] ZENG G, YANG X, YIN A, et al. Simulation of damage evolution and crack propagation in three-point bending pre-cracked asphalt mixture beam[J]. Construction and Building Materials, 2014, 55: 323−332.

[37] ZHOU Xiao-ping, JIA Zhi-ming. The field-enriched finite element methodfornumerical simulationof initiation, propagation and coalescence of multiple cracks[J]. Chinese Journal of Geotechnical Engineering, 2022, 34(6): 988−996.

[38] WONG L N Y, EINSTEIN H H. Crack coalescence in molded gypsum and carrara marble: Part 1. macroscopic observations and interpretation[J]. Rock Mechanics and Rock Engineering, 2009, 42(3): 475−511.

[39] KATAOKA M, OBARA Y, KURUPPU M. Estimation of fracture toughness of anisotropic rocks by semi-circular bend (SCB) tests under water vapor pressure[J]. Rock Mechanics and Rock Engineering, 2015, 48(4): 1353−1367.